# 3D Printed "Earable" Smart Devices for Real-Time Detection of Core Body Temperature

Hiroki Ota,[†,‡] Minghan Chao,[†] Yuji Gao,[†,‡,§] Eric Wu,[†] Li-Chia Tai,[†,‡] Kevin Chen,[†,‡] Yasutomo Matsuoka,[†] Kosuke Iwai,[∥] Hossain M. Fahad,[†,‡] Wei Gao,[†,‡] Hnin Yin Yin Nyein,[†,‡] Liwei Lin,[∥] and Ali Javey*,[†,‡]

†Department of Electrical Engineering & Computer Sciences and ∥Department of Mechanical Engineering, University of California, Berkeley, Berkeley, California 94720, United States

‡Materials Sciences Division, Lawrence Berkeley National Laboratory, Berkeley, California 94720, United States

§Department of Mechanical Engineering, Tianjin University, Tianjin 300072, China

Ⓢ Supporting Information

**ABSTRACT:** Real-time detection of basic physiological parameters such as blood pressure and heart rate is an important target in wearable smart devices for healthcare. Among these, the core body temperature is one of the most important basic medical indicators of fever, insomnia, fatigue, metabolic functionality, and depression. However, traditional wearable temperature sensors are based upon the measurement of skin temperature, which can vary dramatically from the true core body temperature. Here, we demonstrate a three-dimensional (3D) printed wearable "earable" smart device that is designed to be worn on the ear to track core body temperature from the tympanic membrane (i.e., ear drum) based on an infrared sensor. The device is fully integrated with data processing circuits and a wireless module for standalone functionality. Using this smart earable device, we demonstrate that the core body temperature can be accurately monitored regardless of the environment and activity of the user. In addition, a microphone and actuator are also integrated so that the device can also function as a bone conduction hearing aid. Using 3D printing as the fabrication method enables the device to be customized for the wearer for more personalized healthcare. This smart device provides an important advance in realizing personalized health care by enabling real-time monitoring of one of the most important medical parameters, core body temperature, employed in preliminary medical screening tests.

**KEYWORDS:** 3D printing, flexible electronics, wearable device, liquid metal, core body temperature, bone conduction hearing aid
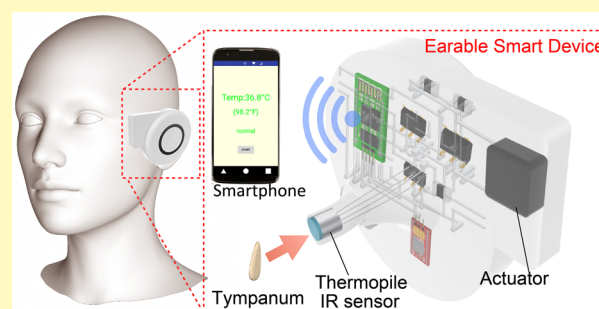
In recent years, the development of wearable smart devices has rapidly expanded,[1−9] targeting applications such as medical,[3] entertainment,[6] biological,[4] and healthcare usage.[1,7−10] In particular, wearable devices for healthcare topics such as exercise,[1,11,12] sleep quality,[13] and preventive medicine[14] have been in high demand. In order to satisfy these demands, many different sensing capabilities such as pressure/strain sensing,[15−17] skin temperature monitoring,[18] pulse oximetry (SpO₂),[19] heart rate monitoring,[19,20] pH sensing,[7] electroencephalogram (EEG) monitoring, and heavy metal detection[8] have been demonstrated.

While most of these sensors have been designed to be worn as a patch, wristband, or headband, here we demonstrate wearable electronics designed to be worn around the ear, which we call an "earable" device. Earable electronics can be worn like headphones and, as such, are ideal for being worn over relatively long periods of time for real-time monitoring of vital signals during exercise as well as for young infants, elderly, and at-risk patients. As individuals' ears can vary significantly in size and shape, we utilize a 3D-printed electronics fabrication scheme using flexible materials to provide personalized earable designs for maximum comfort for long-term use.

As example applications of earable electronics, we demonstrate real-time monitoring of core-body temperature through the tympanum (ear drum) as well as a bone-conduction hearing aid, packaged into a single earable device. The core body temperature is an important indicator of fever,[21] insomnia,[22] fatigue,[23] metabolic functionality,[24] and depression.[25] Currently, most body temperature sensors implemented in wearable devices utilize a resistive-based sensing method for detecting the body surface temperature from the skin.[1,18] While temperature detection from the skin is easy to measure, it can be affected by environmental conditions such as environmental temperature and humidity.[26] On the other hand, while oral, rectal, and organ (tissue) temperature measurements[27] provide more accurate readings of the core body temperature, such
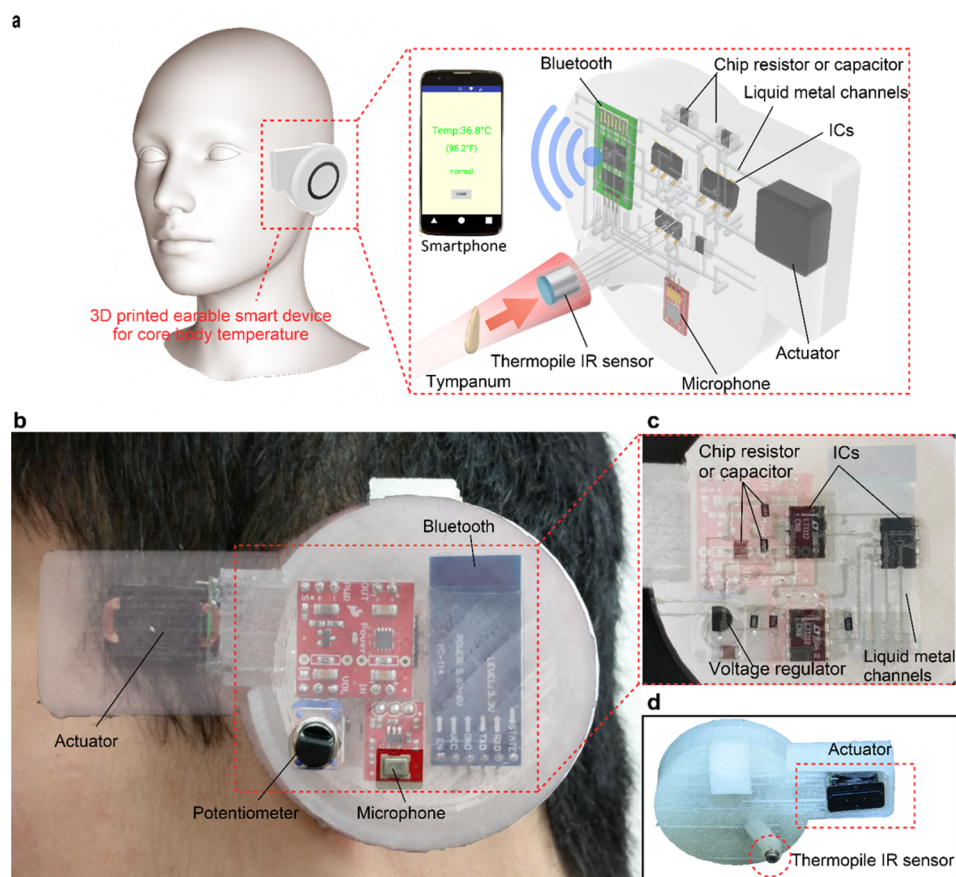
**Figure 1.** 3D printed earable smart device for core body temperature detection. (a) Schematic diagram of the earable smart device, which is composed of a core body temperature detection system using a thermopile IR sensor, a bone conduction hearing aid using an actuator, and a wireless transmission system with a Bluetooth module. (b) Optical image of a subject wearing the smart device. (c) Optical image of the circuitry within the device are overlaid as a reference to the internal circuitry. (d) Angled view of the device showing the bottom with the IR sensor.

measurement techniques are invasive and inappropriate for wearable devices,[26] making the tympanum the optimal location.[28]

## RESULTS AND DISCUSSION

Figure 1a shows a schematic diagram of the device, which is composed of the core body temperature detection system containing a thermopile IR sensor, microphone, bone conducting actuator, integrated circuits (IC) for processing the incoming signals, and a wireless transmission system based on a Bluetooth module. To prevent limitations in hearing due to sound isolation from the thermopile sensor inserted into the ear, a microphone is embedded within the device to capture sound from the outside environment. The sound is then transmitted to the inner ear via bone conduction with an actuator in contact with the temple. The Bluetooth module enables real-time wireless transmission of the core temperature data to a custom built smartphone app (Figure S1). To provide circuit functionality within the flexible earable system and make the process compatible with 3D printing, liquid metal microchannel interconnects using Galinstan metal are used rather than traditional metal wiring (Figure 1b,c,d).[9,29−31]

In order to realize the personalized ear-shaped mold and 3D circuits, a monolithic printing process for 3D embedding of liquid metal (Galinstan) microchannels was performed, as illustrated in Figure 2.[21,32−34] First, a base substrate which fits with individual ear shape and ear canal size is fabricated by a 3D

printer with a stretchable filament (polyurethane). The base substrate contains microchannels for the liquid metal interconnects as well as wells where IC chips can be inserted. After printing, Galinstan is injected into the microchannels and the thermopile sensor, conditioning circuit ICs, and Bluetooth module are inserted into the microchannel slots as the first device layer. Poly(dimethylsiloxane) (PDMS) and epoxy resin are then used to securely set the IC chips in place. As the Bluetooth module is relatively thick (∼7 mm), it takes up space on both the first and second device layers. After curing of the PDMS and epoxy, the second layer containing the components of the bone conduction hearing aid including the microphone, potentiometer, and corresponding conditioning circuits are inserted into their respective microchannel pins. The actuator for the bone conduction is also inserted at this point through the side on the first device layer. Finally, the second layer of devices are also set into place using PDMS and epoxy and a 3D printed enclosure with holes for the microphone and potentiometer is put on to complete the packaging. Figure 1c shows optical images of the two layers of the completed device. As can be seen, the interconnections made by liquid metal also provide a simple pathway for connecting both layers of this multilayer circuit together.

In order to realize the core body temperature detection, the thermopile IR sensor must be properly calibrated to provide an accurate reading. As shown in Figure 3a, the thermopile IR detector is composed of a thermistor and an IR sensor. The thermistor can detect the environmental temperature around a
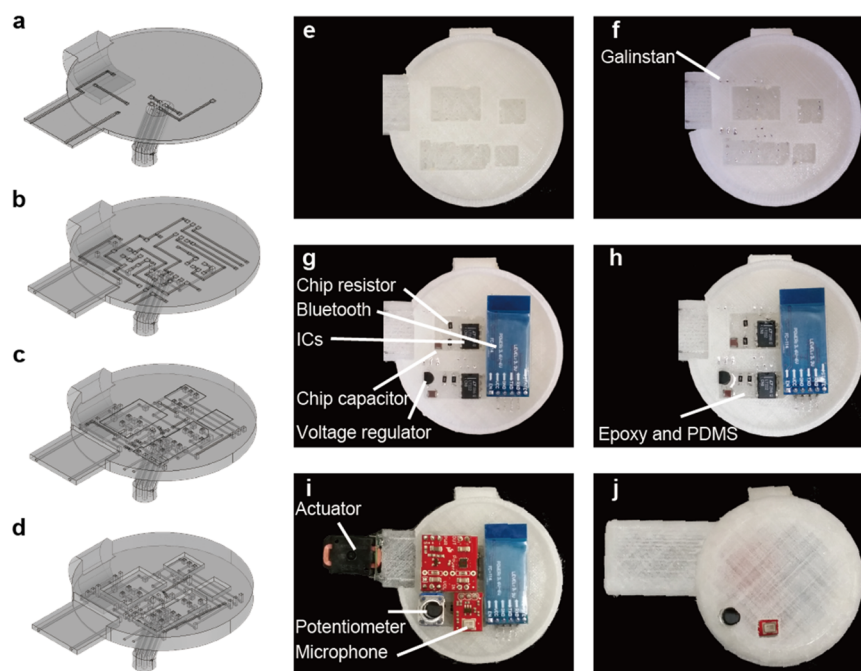
**Figure 2.** Earable device fabrication process. Schematic of the Galinstan channels within the earable device after printing of the first (a), second (b), third (c), and fourth (d) layers. The fabrication process of the smart device (e−j). (e) The base of the device is first 3D printed containing microchannels for the Galinstan interconnects and wells for the ICs. (f) The Galinstan is injected into the microchannels for interconnects. (g) Electrical components for the system are inserted into the wells. (h) Epoxy and PDMS are poured onto the wells in order to securely set the components in place. (i) The actuator, potentiometer, and other components for the bone conduction hearing aid are inserted. (j) A 3D printed enclosure with holes for the microphone and potentiometer is put on to complete the packaging.
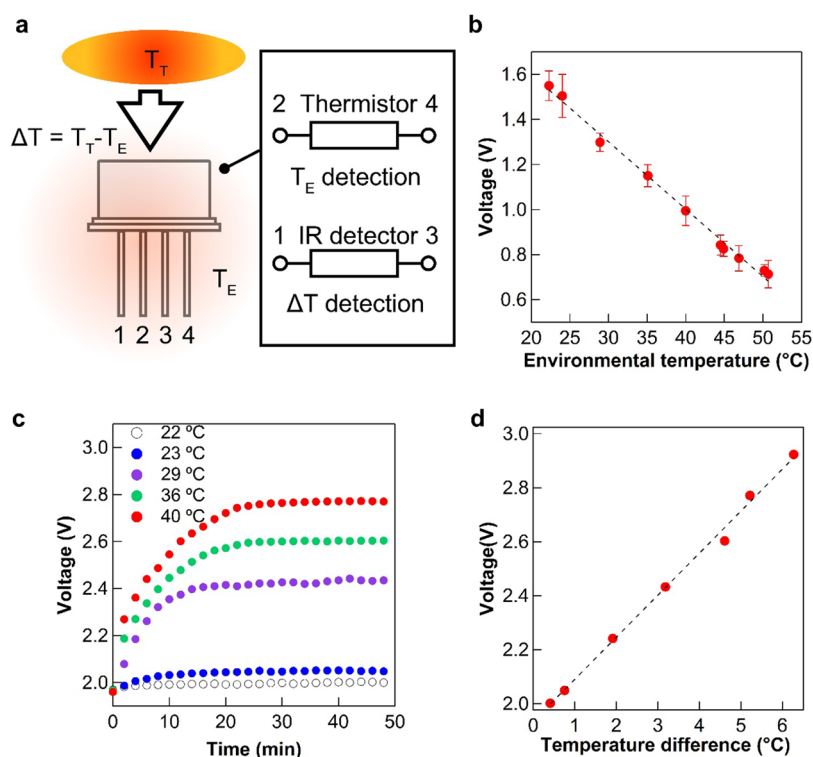


**Figure 3.** Thermopile IR sensor calibration. (a) Schematic demonstrating the mechanism of temperature detection in the thermopile IR sensor. (b) Output voltage of the thermistor in the thermopile IR sensor versus environmental temperature. (c) Output voltage of the IR detector in the thermopile IR sensor as a function of time as the temperature is ramped to different set points. (d) Calibrated output voltage of the IR sensor as a function of the temperature difference between the IR sensor and thermistor.

thermopile IR detector ($T_E$) while the IR sensor detects the temperature difference ($\Delta T$) between $T_E$ and temperature of

the target ($T_T$). For the thermistor, the resistance change with temperature is converted into a voltage by using a voltage
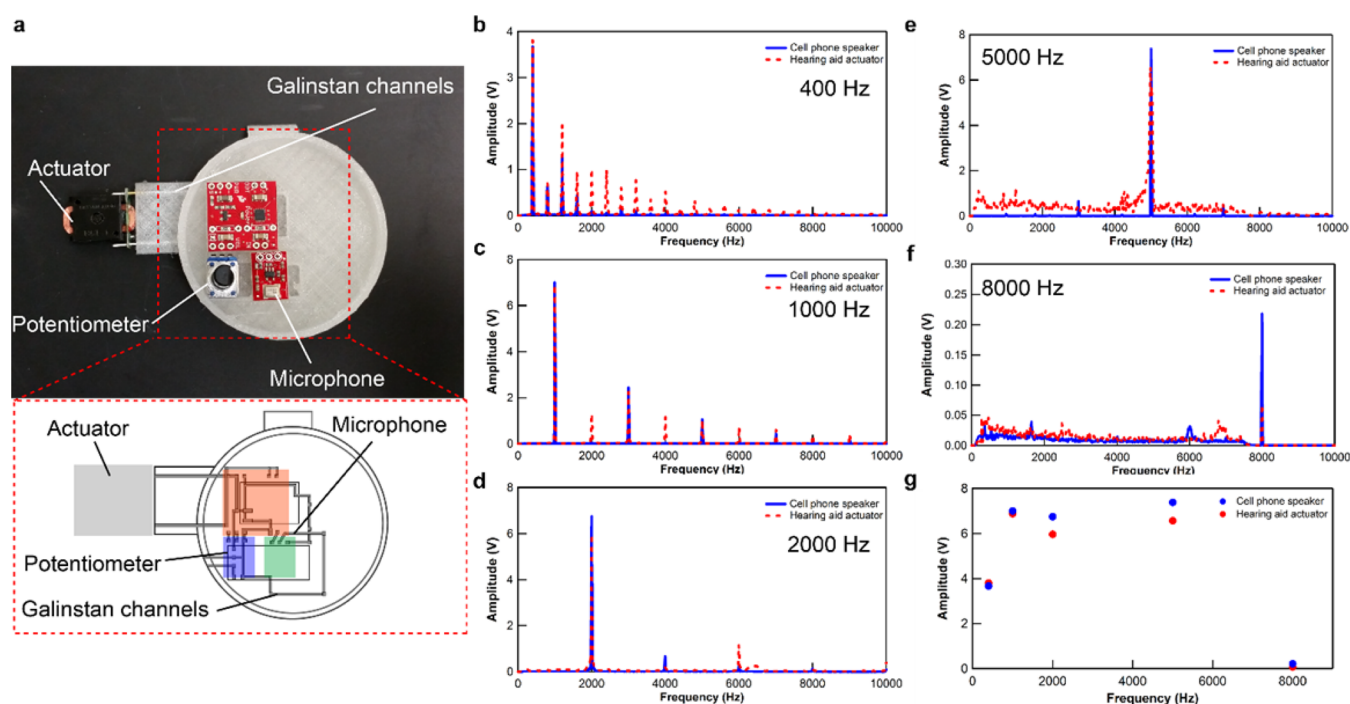
**Figure 4.** Bone-conduction hearing aid characterization. (a) Optical image and a corresponding schematic diagram of the bone-conduction hearing aid. (b−f) Frequency analysis of sound conduction via the hearing aid actuator compared to a cell phone speaker for (b) 400 Hz, (c) 1000 Hz, (d) 2000 Hz, (e) 5000 Hz, and (f) 8000 Hz. (g) Amplitude as a function of frequency for the hearing aid actuator and cell phone speaker.
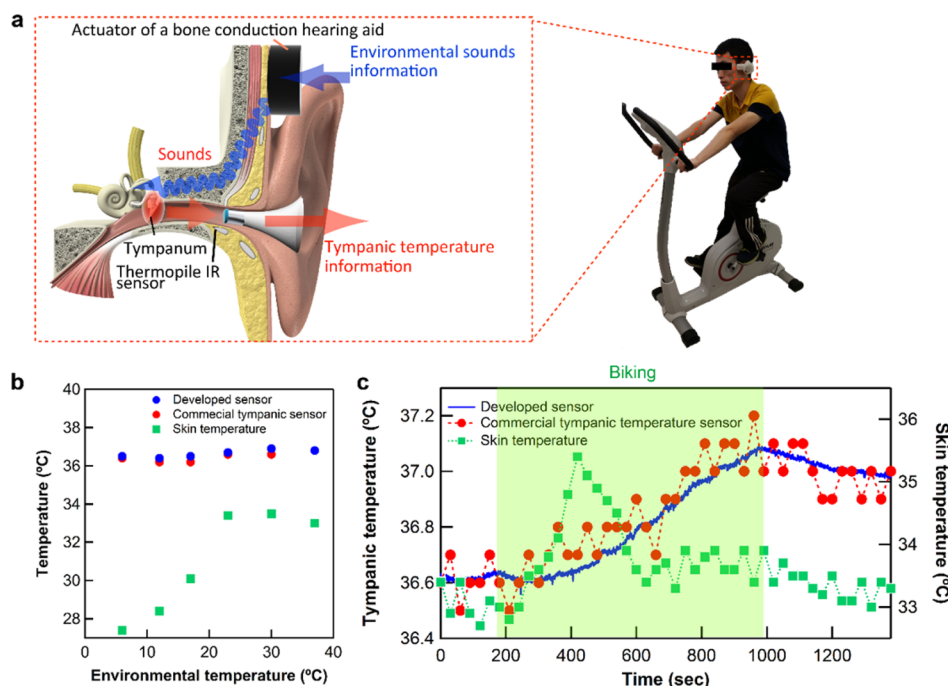


**Figure 5.** On-body tests using the 3D printed earable smart device. (a) Schematic diagram of the smart device operation. (b) Skin and core body temperatures as a function of environmental temperature. (c) Skin and core body temperature change during biking.

divider (Figure S2 and S3). Figure 3b and Figure S4 shows the experimental as well as simulated voltage output of the thermistor (Discussion S1) versus temperature $T_E$, indicating a good linear response between 24 and 50 °C. In order to calibrate the IR detector in the thermopile IR sensor, a test structure imitating the ear canal was fabricated using 3D printing (Figure S5). The structure contains a microchannel resistive heater using silicon oil containing silver microparticles

as the heating element.[9] Figure 3c shows the change in output voltage of the IR detector as a function of time for different temperatures confirmed by a commercial thermocouple. In order to get a calibration curve for the IR detector, the temperature difference, $\Delta T$, between $T_E$ and $T_T$ was calculated based on the temperature indicated by the thermocouple and the one calculated from Figure 2b. Figure 2d shows the calculated $\Delta T$ and voltage from the IR detector. The

relationship between the $\Delta T$ and the IR detector output voltage is approximately linear from 20 to 50 °C. Based on the calibration experiments, the relationship between the temperatures and output voltages measured by the thermistor and IR detector is as follows:

$$T_E = V_{TM} \times (-33.4) + 73.5$$

$$\Delta T = (V_{IR} - 1.9) \times 6.4$$

$$T_T = T_E + \Delta T$$

Figure 4a shows a bone-conduction hearing aid, which is composed of a microphone, data processing circuitry, a potentiometer for adjusting volume, an actuator for transmitting sound via bone conduction, and Galinstan channels for the interconnects (Figures S6 and S7). While the forehead is able to conduct sound better than the temple,[35] the temple was selected so that both the hearing aid and core temperature sensor could be integrated together in one device. Figure 4b−f shows the frequency analysis of sound conduction measured by contacting the actuator to a PC microphone compared to the frequency analysis of sound transmitted through air via a cell phone speaker using reference tones at 400, 1000, 2000, and 5000 Hz (Figure S8). The amplitude as a function of frequency was obtained by Fast Fourier Transform (FFT) conversion from the signal received from the microphone of a commercial PC. Figure 4g indicates the amplitudes of each reference tone as a function of wavelength. As shown in Figure 4g, the frequency range of the hearing aid actuator is similar to that of a normal speaker up to approximately 5000 Hz (percentage of amplitude at 400, 1000, 2000, and 5000 Hz with respect to the cell phone speaker is 103%, 98%, 88%, and 89%), and sharply drops to 31% with respect to the cell phone speaker at 8000 Hz due to limitations in the transducer, which is in line with most bone conduction hearing aids.[36,37]

On-body testing was performed with the 3D printed smart earable device containing the thermopile IR sensor for core body temperature detection and bone-conduction hearing aid (Figure 5a). To test the effect of environmental temperature on the readings, a subject was placed in rooms heated or cooled down to various temperatures ranging from 6 to 40 °C. Figure S9 shows the core body temperature measured by the earable sensor and a commercial tympanic sensor as well as the skin temperature on a subject's arm measured by an IR noncontact thermometer versus the environmental temperature. While the skin temperature is heavily influenced by the temperature of the environment, the core body temperature is nearly constant, as measured by both our earable sensor and the commercial tympanic sensor. This reflects the inability of skin temperature measurements to provide a true temperature reading that accurately reflects the health state of a subject. Figure 5b indicates the relationship between the environmental temperature in each room and the measured core body/skin temperature 200 s after entering each room. In rooms kept below 23 °C, the skin temperature decreases while the core body temperature stays constant during measurement. In the rooms set to 23 and 30 °C, the core body and skin temperatures both stay approximately constant during measurement. In the case of the 40 °C room, the skin temperature increased at first, but decreased gradually after a few minutes. At this temperature, sweating was observed during measurement, which might lead to cooling of the skin temperature.[26,38]

In addition to environmental testing, the temperature change due to exercise was also analyzed, as depicted in Figure 5c. Real time tympanic core body temperature was measured continuously by the earable sensor worn by the subject on the left ear while reference temperature measurements were taken every 30 s by a commercial tympanic sensor. In addition, the skin temperature from the forearm was measured every 30 s using an IR sensor. Initially, the subject maintained at rest for 3 min to obtain a baseline "at rest" reading of approximately 36.6 °C core body temperature and 33.5 °C skin temperature. After rest, the subject began to bike on a cycling ergometer for approximately 13.5 min. Over the course of exercise, the core body temperature rises steadily up to approximately 37 °C by the end of biking while the skin temperature rises quickly to approximately 35 °C before dropping back down. The drop in the skin temperature is in good agreement with other reports,[1,37,39] and can be attributed to perspiration during exercise. After conclusion of exercise, the tympanic temperature begins to slowly drop back down. As can be seen, our earable core body temperature detector stays in excellent agreement with the core body temperature measured by the commercial tympanic sensor, regardless of environmental or physical conditions, providing a much more reliable real-time measurement of an individual's health and physiological state as compared to simple skin temperature measurements.

## ■ CONCLUSIONS

We have demonstrated a 3D printed earable smart device for core body temperature detection with an integrated bone conduction hearing aid. The 3D printing technique using liquid metal interconnects allows for more personalized smart devices tuned to fit the needs and comfort of individual users. The functionality of the sensor was verified by operating it in different environmental conditions as well as different physical states of subjects, confirming that unlike skin temperature sensors, it is not affected by any such external perturbations. Here, the size of the earable device is limited by the resolution of our printer (300 $\mu$m minimum microchannel wdith) and size of off-the-shelf thermopile sensor and ICs (few millimeters to centimeter scale). In the future, with more advanced 3D printers and by using custom-designed ICs, the size of the system can be further reduced. While only a bone-conduction hearing aid and tympanic sensor were demonstrated in this work, sensors for measuring other vital signals such as heart rate, pule oximetry, and EEG may also be integrated into the 3D printed earable device platform for comprehensive long-term, real-time monitoring of an individual's health and physiological state.

## ■ EXPERIMENTAL SECTION

**3D Printing.** The 3D computer-aided design (CAD) data for the devices were created with AutoCAD 2014 (Autodesk Inc.) The STL file converted from the 3D CAD data was used by the Simplify3D software (Simplify3D) to conduct the 3D printing. The stretchable 3D material (Filaflex, Recreus) was printed using an M2 3D printer (M2 printer, MakerGear) with a nozzle diameter of 350 $\mu$m. Printing of each layer (100 $\mu$m thickness) was conducted at a speed of 1500 mm/min with the hot-end set to 246 °C and the stage at 45 °C. After 3D printing of the substrate, liquid metal (Galinstan, Rotometal) was injected into microchannels. Then, electronic components including a thermopile IR sensor and Bluetooth module were inserted into the microchannels. Components were connected with via liquid metal wire. In order to make top surfaces flat, and set the components in

place, PDMS and epoxy were poured into the wells containing the components.

**Signal Conditioning, Processing, and Wireless Transmission Circuit Design of Thermopile IR Sensor.** The circuit diagram of the analog signal-conditioning block of the earable device is shown in Figure S3. The thermopile IR sensor (HMS-J11 F5.5, HEIMANN sensor) generates two sensor signals: one is the IR detector voltage and the other is the thermistor resistance change.

The IR detector voltage outputs in the hundreds of microvolts range and the resolution is several microvolts, so an LT1112 op amp (Linear technology) is chosen due to its low input voltage noise. In addition, the LT1112 provides two op amps in one Dual In-Line Package (DIP), which saves space with minimal pin numbers. The IR detector voltage is amplified by a noninverting amplifier topology with the specific resistors feedback (1 M ohm and 1k ohm) to provide a gain of 1001. The virtual ground in the noninverting amplifier is buffered with a voltage follower in order to reduce the output impedance and make the virtual ground capable of sourcing and sinking currents. The amplified signal is then sent to the microcontroller for analog-to-digital (ADC) conversion. The resistance change of the thermistor is converted into a voltage by adopting a voltage divider configuration. As the thermistor resistance is approximately 120 kΩ, a 120 kΩ resistor is used to set the output voltage at approximately half of the supply voltage. The voltage is buffered by a voltage follower to lower the output impedance and eliminate error due to the finite input impedance of the microcontroller ADC. The buffered voltage signal is then sent to the microcontroller, which is an ATtiny85 (Atmel 8-bit) (Atmel) microcontroller in DIP that is programmed by a pocket AVR programmer from SparkFun beforehand. Signals from the sensor module were conditioned by our analog circuitry and then relayed to the Bluetooth transceiver using the Universal Asynchronous Receiver/ Transmitter (UART) protocol. The Bluetooth then communicates with the mobile phone wirelessly to send the data.

**Power Delivery to the Device of Body Temperature Sensor.** The earable device is powered by a single rechargeable lithium-ion polymer battery with a nominal voltage of 3.7 V. The equivalent diagram is shown in Figure S10. The nominal 3.7 V voltage is regulated by an LP2950 3.3 V linear voltage regulator due to its high efficiency and extremely low quiescent power dissipation. The Bluetooth is powered by 3.7 V battery and all of the remaining circuit components are powered by the regulated 3.3 V. The total power dissipation of the entire circuit is less than 30 mW.

**Heating Device for Calibration of Thermopile Sensor.** The basic device concept of the 3D printed heating device for temperature calibration is the same as the resistive heater in a previous report.[9] The structure of the heating device (Figure S5) was fabricated by a 3D printer (Creatr HS, Leapfrog) using polylactic acid (PLA). Printing of each layer was conducted at a speed of 3000 mm/min with the hot-end set to 225 °C and the stage set to 45 °C. All other printing parameters used are the same as the M2 printer. After printing, silicone oil containing 70% silver microparticles (AgMP, Sigma-Aldrich) was injected in a spiral channel. The temperature inside the device was controlled by applying different voltages to the channel. The inside temperature was monitored with a thermometer.

**Signal Conditioning, Processing Circuit Design of Bone-Conduction Hearing Aid.** The bone-conduction hearing aid circuit contains three parts:

1. The first part is a MEMS microphone breakout board from Sparkfun. The board functions as the preamplifier for the microphone. The key part is the ADMP401 chip. It is a high-quality low-power MEMS microphone chip containing an impedance converter and an output amplifier. Its high SNR (signal-to-noise ratio) of 62 dB improves the sound quality and provides a flat frequency response from 100 Hz to 15 kHz, allowing sufficient bandwidth for sound. Thus, the sound signal can be properly amplified and converted to an analog voltage signal without much distortion. The rest of the circuit uses the op amp OPA334 to further amplify and filter the analog voltage signal.

2. The second part is a mono audio amplifier breakout board from Sparkfun. The board functions as the class-D amplifier. The key part of the board is a TPA2005D1RB chip, which is a mono filter-free class-D audio power amplifier. It takes in the analog voltage output from the MEMS microphone breakout board and filters it through an RC circuit. The shutdown pin enables the generation of a 250 kHz PWM-like signal to the output. The PWM-like output drives a speaker typically, but in this project, it drives a bone conducting actuator at the output. A potentiometer (10 kΩ max) is connected at the input of the breakout board. It can be turned manually to adjust the amplitude of the signal to control the sound volume.

3. The third part is a bone conducting exciter (BCE-1) from Dayton. The audio exciter produces sound through direct vibration of actuators and transmits the sound through the temple. It effectively acts like a speaker, but with different mechanism of creating sound.

**Frequency Analysis of Sound Conduction by Actuator and Air.** The frequency analysis was performed by FFT conversion of the signal from the microphone of a PC using software (X recorder, Wat). Reference sounds are generated from the speaker of a smartphone (Galaxy S4, Samsung). For the reference frequency distribution (sound conduction via air), the microphone of a PC received sound from the speaker of a smartphone. On the other hand, the frequency distribution of the actuator was obtained by contacting the actuator with the PC microphone. The signal data from microphone was converted into frequency data with FFT.

**The Custom Mobile Application Design of Mobile Display.** A mobile application (Earable device app) was designed to provide a user-friendly interface for receiving and displaying transmitted data in real time (Figure S1). The data conversion from voltage to temperature is done based on the calibration curve. The application is capable of displaying the temperature in real time. According to the body temperature data received, the application can show if the user's body temperature is normal, too cold, in a fever, or in danger. The color of the display also changes according to the temperature in order to provide better visualization of the change in body temperature. Although the current application is only implemented in the Android environment, a similar application can also be developed for other popular mobile operating systems such as iOS in the future.

**On-Body Test in Different Temperature Conditions and during Biking.** In order to observe the difference between skin and core body temperature change, a subject wearing the smart device was asked to stay in rooms set at different temperatures (6, 12, 17, 23, 30, and 40 °C). During on-body tests, the reference core body temperature was measured by a commercial IR ear thermometer. The skin temperature was measured by a commercial IR thermometer (BENETEC GM550, Noza Tec).

To conduct the biking test, a subject wearing the earable device first sat at rest on an air-bike to obtain a baseline temperature reading, started biking 180 s later at a cycling power of 50 W, and stopped at 1000 s. The measurement of core body temperature and skin temperature of the subject was performed in same manner as on-body test in different temperature conditions.

## ■ ASSOCIATED CONTENT

### Ⓢ Supporting Information

The Supporting Information is available free of charge on the ACS Publications website at DOI: 10.1021/acssensors.7b00247.

> Custom-developed mobile application; system-level block diagrams of the thermopile IR sensor and bone-conduction hearing aid, and circuit diagrams of the signal-conditioning circuit of the thermopile IR sensor and bone-conduction hearing aid; relationship between temperature and voltage of the thermistor; 3D printed heating device for temperature calibration; discussion: output voltage simulation of the thermistor voltage divider (PDF)

## ■ AUTHOR INFORMATION

**Corresponding Author**
*E-mail: ajavey@eecs.berkeley.edu.
**ORCID** Ⓘ
Kevin Chen: 0000-0002-6726-6132
Ali Javey: 0000-0001-7214-7931

**Author Contributions**

H. O. collected all data and led all experiments. M. C. developed the data processing circuit for the thermopile IR sensor and fabricated the smart device. Y. G. helped with the experimental setup of 3D printing, and device fabrication. E. W. helped with the circuit design for the thermopile IR sensor. L. T. helped with the 3D printing. K. C. helped construct the electrical setup. Y. M. developed the design for the bone-conduction hearing aid device. K. I. helped with the temperature measurement in cold/warm/hot rooms. H. M. F., W. G., and H. Y. Y. N. helped with the design of experiments. H. M. F. helped with the electrical set-ups and circuit development. W. G. and H. Y. Y. N. helped set up and design the biking experiments. L. L. guided the experiments for temperature measurement in cold/warm/hot rooms. A. J. guided the research. H. O., M. C., K. C., and A. J. wrote the paper.

**Notes**

The authors declare no competing financial interest.

## ■ ACKNOWLEDGMENTS

## ■ REFERENCES

(1) Gao, W.; Emaminejad, S.; Nyein, H. Y. Y.; Challa, S.; Chen, K.; Peck, A.; Fahad, H. M.; Ota, H.; Shiraki, H.; Kiriya, D.; et al. Fully Integrated Wearable Sensor Arrays for Multiplexed in Situ Perspiration Analysis. *Nature* **2016**, *529*, 509−514.

(2) Ota, H.; Chen, K.; Lin, Y.; Kiriya, D.; Shiraki, H.; Yu, Z.; Ha, T.-J.; Javey, A. Highly Deformable Liquid-State Heterojunction Sensors. *Nat. Commun.* **2014**, *5*, 5032.

(3) Xu, S.; Zhang, Y.; Jia, L.; Mathewson, K. E.; Jang, K.-I.; Kim, J.; Fu, H.; Huang, X.; Chava, P.; Wang, R.; et al. Soft Microfluidic Assemblies of Sensors, Circuits, and Radios for the Skin. *Science* **2014**, *344*, 70−74.

(4) Jeong, J.-W.; McCall, J. G.; Shin, G.; Zhang, Y.; Al-Hasani, R.; Kim, M.; Li, S.; Sim, J. Y.; Jang, K.-I.; Shi, Y.; et al. Wireless Optofluidic Systems for Programmable In Vivo Pharmacology and Optogenetics. *Cell* **2017**, *162*, 662−674.

(5) Matsuhisa, N.; Kaltenbrunner, M.; Yokota, T.; Jinno, H.; Kuribara, K.; Sekitani, T.; Someya, T. Printable Elastic Conductors with a High Conductivity for Electronic Textile Applications. *Nat. Commun.* **2015**, *6*, 7461.

(6) Prattichizzo, D.; Chinello, F.; Pacchierotti, C.; Malvezzi, M. Towards Wearability in Fingertip Haptics: A 3-DoF Wearable Device for Cutaneous Force Feedback. *IEEE Transactions on Haptics* **2013**, *6*, 506−516.

(7) Nyein, H. Y. Y.; Gao, W.; Shahpar, Z.; Emaminejad, S.; Challa, S.; Chen, K.; Fahad, H. M.; Tai, L.-C.; Ota, H.; Davis, R. W.; et al. A Wearable Electrochemical Platform for Noninvasive Simultaneous Monitoring of Ca2+ and pH. *ACS Nano* **2016**, *10*, 7216−7224.

(8) Gao, W.; Nyein, H. Y. Y.; Shahpar, Z.; Fahad, H. M.; Chen, K.; Emaminejad, S.; Gao, Y.; Tai, L.-C.; Ota, H.; Wu, E.; et al. Wearable Microsensor Array for Multiplexed Heavy Metal Monitoring of Body Fluids. *ACS Sens.* **2016**, *1*, 866−874.

(9) Ota, H.; Emaminejad, S.; Gao, Y.; Zhao, A.; Wu, E.; Challa, S.; Chen, K.; Fahad, H. M.; Jha, A. K.; Kiriya, D.; et al. Application of 3D Printing for Smart Objects with Embedded Electronic Sensors and Systems. *Advanced Materials Technologies* **2016**, *1*, 1600013.

(10) Wu, S.-Y.; Yang, C.; Hsu, W.; Lin, L. 3D-Printed Microelectronics for Integrated Circuitry and Passive Wireless Sensors. *Microsystems & Nanoengineering* **2015**, *1*, 15013.

(11) Bandodkar, A. J.; Jia, W.; Yardımcı, C.; Wang, X.; Ramirez, J.; Wang, J. Tattoo-Based Noninvasive Glucose Monitoring: A Proof-of-Concept Study. *Anal. Chem.* **2015**, *87*, 394−398.

(12) Mengüç, Y.; Park, Y.−L.; Villalpando, E.; Aubin, P.; Zisook, M.; Stirling, L.; Wood, R. J.; Walsh, C. J. Soft Wearable Motion Sensing Suit for Lower Limb Biomechanics Measurements; IEEE International Conference on Robotics and Automation (ICRA), 2013; pp 5289−5296.

(13) Choi, S.; Jiang, Z. A Novel Wearable Sensor Device with Conductive Fabric and PVDF Film for Monitoring Cardiorespiratory Signals. *Sens. Actuators, A* **2006**, *128*, 317−326.

(14) Axisa, F.; Schmitt, P. M.; Gehin, C.; Delhomme, G.; McAdams, E.; Dittmar, A. Flexible Technologies and Smart Clothing for Citizen Medicine, Home Healthcare, and Disease Prevention. *IEEE Transactions on Information Technology in Biomedicine* **2005**, *9*, 325−336.

(15) Lipomi, D. J.; Vosgueritchian, M.; Tee, B. C.-K.; Hellstrom, S. L.; Lee, J. A.; Fox, C. H.; Bao, Z. Skin-like Pressure and Strain Sensors Based on Transparent Elastic Films of Carbon Nanotubes. *Nat. Nanotechnol.* **2011**, *6*, 788−792.

(16) Muth, J. T.; Vogt, D. M.; Truby, R. L.; Mengüç, Y.; Kolesky, D. B.; Wood, R. J.; Lewis, J. A. Embedded 3D Printing of Strain Sensors within Highly Stretchable Elastomers. *Adv. Mater.* **2014**, *26*, 6307−6312.

(17) Park, Y. − L.; Majidi, C.; Kramer, R.; Bérard, P.; Wood, R. J. Hyperelastic pressure sensing with a liquid-embedded elastomer. *J. Micromech. Microeng.* **2010**, *20*, 125029.

(18) Webb, R. C.; Bonifas, A. P.; Behnaz, A.; Zhang, Y.; Yu, K. J.; Cheng, H.; Shi, M.; Bian, Z.; Liu, Z.; Kim, Y.-S.; et al. Ultrathin Conformal Devices for Precise and Continuous Thermal Characterization of Human Skin. *Nat. Mater.* **2013**, *12*, 938−944.

(19) Yokota, T.; Zalar, P.; Kaltenbrunner, M.; Jinno, H.; Matsuhisa, N.; Kitanosako, H.; Tachibana, Y.; Yukita, W.; Koizumi, M.; Someya, T. Ultraflexible Organic Photonic Skin. *Sci. Adv.* **2016**, *2*, e1501856.

(20) Kim, D.-H.; Lu, N.; Ma, R.; Kim, Y.-S.; Kim, R.-H.; Wang, S.; Wu, J.; Won, S. M.; Tao, H.; Islam, A.; et al. Epidermal Electronics. *Science* **2011**, *333*, 838.

(21) Nakamura, K. Central Circuitries for Body Temperature Regulation and Fever. *Am. J. Physiol Regul Integr Comp Physiol* **2011**, *301*, R1207.

(22) Murphy, P. J.; Campbell, S. S. Nighttime drop in body temperature: a physiological trigger for sleep onset? *Sleep* **1997**, *20*, 505−511.

(23) Hamilos, D. L.; Nutter, D.; Gershtenson, J.; Redmond, D. P.; Di Clementi, J. D.; Schmaling, K. B.; Make, B. J.; Jones, J. F. Core Body Temperature Is Normal in Chronic Fatigue Syndrome. *Biol. Psychiatry* **1998**, *43*, 293−302.

(24) Geiser, F. Metabolic Rate and Body Temperature Reduction During Hibernation and Daily Torpor. *Annu. Rev. Physiol.* **2004**, *66*, 239−274.

(25) Szuba, M. P.; Guze, B. H.; Baxter, L. R., Jr. Electroconvulsive Therapy Increases Circadian Amplitude and Lowers Core Body Temperature in Depressed Subjects. *Biol. Psychiatry* **1997**, *42*, 1130−1137.

(26) Winslow, C. − E. A.; Herrington, L. P.; Gagge, A. P. Physiological reactions of the human body to varying environmental temperatures. *Am. J. Physiol.* **1937**, *120*, 1−21.

(27) Sund-Levander, M.; Forsberg, C.; Wahren, L. K. Normal Oral, Rectal, Tympanic and Axillary Body Temperature in Adult Men and Women: A Systematic Literature Review. *Scandinavian Journal of Caring Sciences* **2002**, *16*, 122−128.

(28) Shinozaki, T.; Deane, R.; Perkins, F. M. Infrared Tympanic Thermometer: Evaluation of a New Clinical Thermometer. *Crit. Care Med.* **1988**, *16*, 148−150.

(29) Adams, J. J.; Duoss, E. B.; Malkowski, T. F.; Motala, M. J.; Ahn, B. Y.; Nuzzo, R. G.; Bernhard, J. T.; Lewis, J. A. Conformal Printing of Electrically Small Antennas on Three-Dimensional Surfaces. *Adv. Mater.* **2011**, *23*, 1335−1340.

(30) Lewis, J. A.; Ahn, B. Y. Device fabrication: Three-dimensional printed electronics. *Nature* **2015**, *518*, 42−43.

(31) Palleau, E.; Reece, S.; Desai, S. C.; Smith, M. E.; Dickey, M. D. Self-Healing Stretchable Wires for Reconfigurable Circuit Wiring and 3D Microfluidics. *Adv. Mater.* **2013**, *25*, 1589−1592.

(32) Dickey, M. D.; Chiechi, R. C.; Larsen, R. J.; Weiss, E. A.; Weitz, D. A.; Whitesides, G. M. Eutectic Gallium-Indium (EGaIn): A Liquid Metal Alloy for the Formation of Stable Structures in Microchannels at Room Temperature. *Adv. Funct. Mater.* **2008**, *18*, 1097−1104.

(33) Zhu, S.; So, J.-H.; Mays, R.; Desai, S.; Barnes, W. R.; Pourdeyhimi, B.; Dickey, M. D. Ultrastretchable Fibers with Metallic Conductivity Using a Liquid Metal Alloy Core. *Adv. Funct. Mater.* **2013**, *23*, 2308−2314.

(34) Mannoor, M. S.; Jiang, Z.; James, T.; Kong, Y. L.; Malatesta, K. A.; Soboyejo, W. O.; Verma, N.; Gracias, D. H.; McAlpine, M. C. 3D Printed Bionic Ears. *Nano Lett.* **2013**, *13*, 2634−2639.

(35) McBride, M.; Tran, P.; Letowski, T.; Patrick, R. The Effect of Bone Conduction Microphone Locations on Speech Intelligibility and Sound Quality. *Applied Ergonomics* **2011**, *42*, 495−502.

(36) Park, H.-W.; Kim, M.-S.; Bae, M.-J. Improvement of Voice Quality and Prevention of Deafness by a Bone-Conduction Device. *Biotechnol. Biotechnol. Equip.* **2014**, *28*, S14−S20.

(37) Christensen, L.; Smith-Olinde, L.; Kimberlain, J.; Richter, G. T.; Dornhoffer, J. L. Comparison of traditional bone-conduction hearing AIDS with the Baha system. *J. Am. Acad. Audiol* **2010**, *21*, 267−73.

(38) Torii, M.; Yamasaki, M.; Sasaki, T.; Nakayama, H. Fall in Skin Temperature of Exercising Man. *Br. J. Sports Med.* **1992**, *26*, 29−32.

(39) Fernandes, A. A.; Amorim, P. R.; Brito, C. J.; de Moura, A. G.; Costa, C. M.; Sillero, M.; Marins, J. C. Measuring skin temperature before, during and after exercise: a comparison of thermocouples and infrared thermography. *Physiol. Meas.* **2014**, *35*, 189.

# Supporting Information
# 3D Printed Earable Smart Devices
# for Real-time Detection of Core Body Temperature

Hiroki Ota[1,2], Minghan Chao[1], Yuji Gao[1,2,3], Eric Wu[1], Li-Chia Tai[1,2], Kevin Chen[1,2],

Yasutomo Matsuoka[1], Kosuke Iwai[4], Hossain M. Fahad[1,2], Wei Gao[1,2], Hnin Yin Yin

Nyein[1,2], Liwei Lin[4], and Ali Javey[1,2]*


[1]Department of Electrical Engineering & Computer Sciences, University of California, Berkeley,

CA

[2]Materials Sciences Division, Lawrence Berkeley National Laboratory, Berkeley, CA

[3]Department of Mechanical Engineering, Tianjin University, Tianjin, China

[4]Department of Mechanical Engineering, University of California, Berkeley, CA

*Correspondence should be addressed to A.J. (ajavey@eecs.berkeley.edu)

**Table of contents:**

**Fig. S1. The custom-developed mobile application for data display**

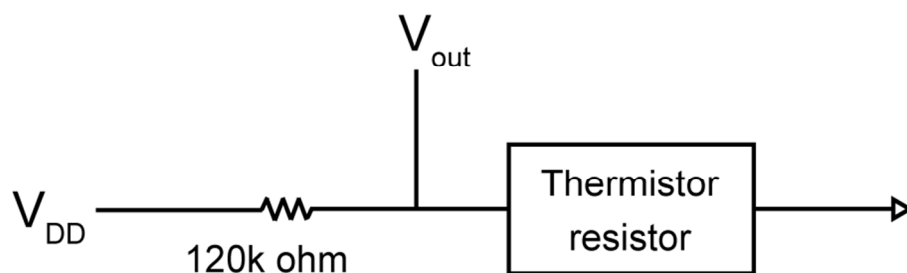**Fig. S2. System-level block diagram of the thermopile IR sensor.**

**Fig. S3. Circuit diagram of the signal-conditioning circuit for the thermopile IR sensor**
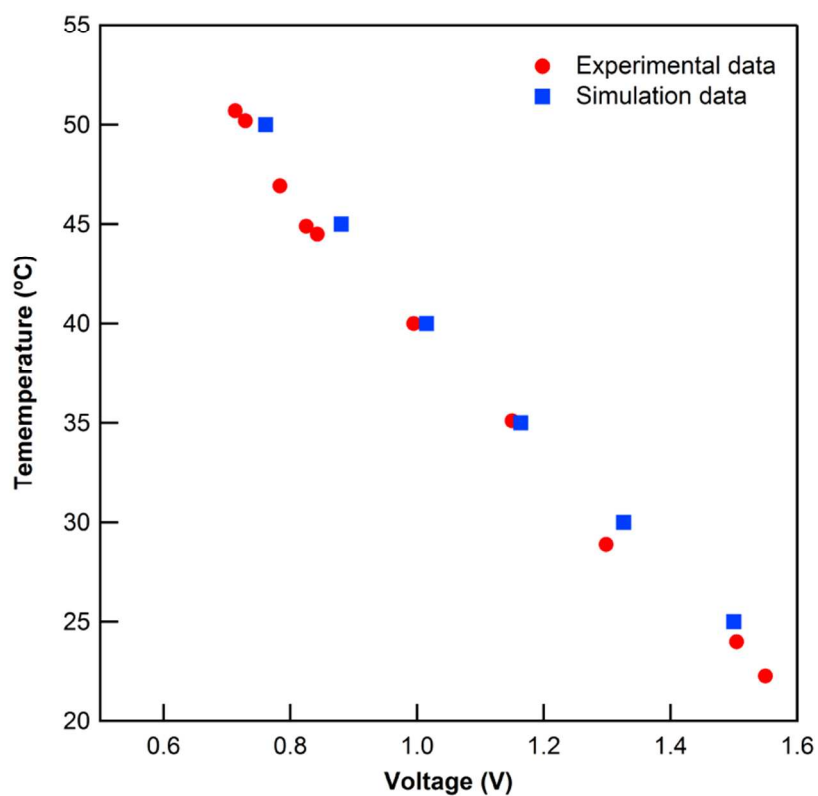
**a**



**b**



**Fig. S4. Relationship between temperature and voltage of the thermistor.**
**a**. Equivalent circuit diagram for the thermistor voltage divider circuit. **b.** Experimental and simulated output voltage of the thermistor voltage divider for temperatures from 20 °C to 55 °C.

**Discussion. S1. Output voltage simulation of the thermistor voltage divider**

For the simulation, the nominal thermistor resistance vs. temperature data in the thermopile IR sensor datasheet was used. According to the datasheet, the relation between the thermistor resistance and temperature is non-linear. Thus, in order to linearize the relationship, the thermistor is connected in series with a normal resistor to form a voltage-divider circuit. As a result, the output voltage becomes approximately linear over the temperature range of interest. In this application, a 120 kΩ resistor is used for the normal resistor because the nominal thermistor resistance at room temperature (20 °C) is around 120 kΩ. With almost equal resistances in the voltage-divider circuit, the linear region is centered in the range of interest, thus the linearization effect is more significant. The output voltage reflects the thermistor resistance change. The relation between output voltage and the thermistor resistance is captured by the following equation.

$$V_{out} = \frac{R_{thermistor}}{R_{thermistor} + 120k\Omega} \times V_{DD}$$

**a**

Thermometer    Applied voltage

70% Silver micro-particle in silicon oil

Thermopile IR sensor

**b**

Power

Heating device

Themometer

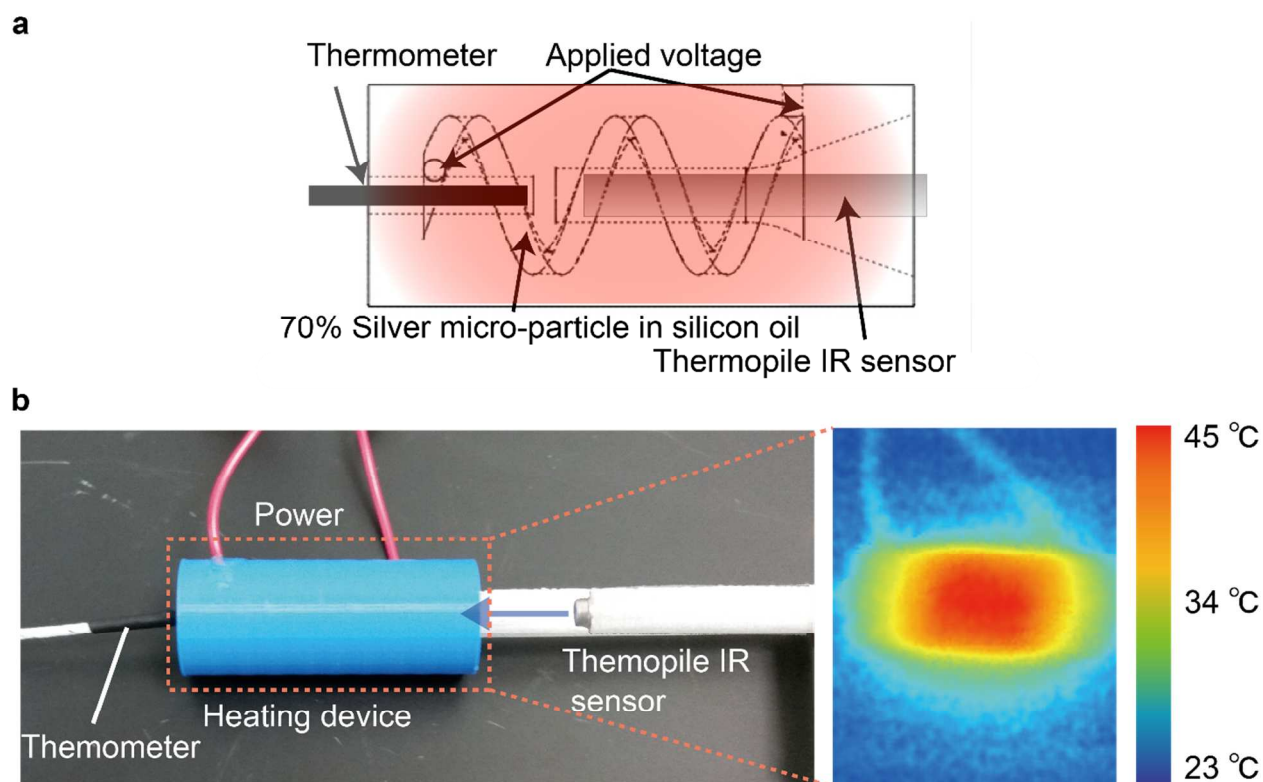Themopile IR sensor

45 °C

34 °C

23 °C

**Fig. S5. 3D printed heating device for temperature calibration.** (a) Schematic diagram of the 3D printed heating device used to calibrate the thermopile IR sensor. (b) Optical image of the testing setup and IR camera image of the temperature profile in the device.
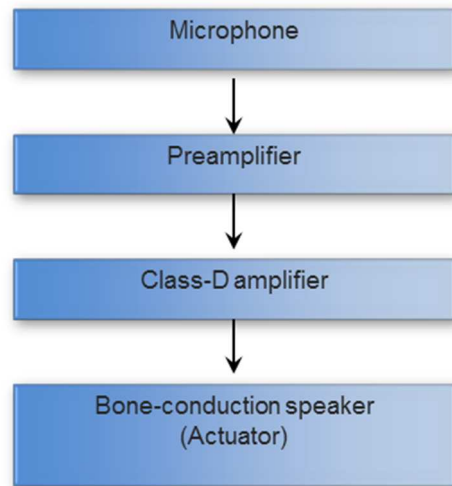
**Fig. S6. System-level block diagram of the bone-conduction hearing aid**
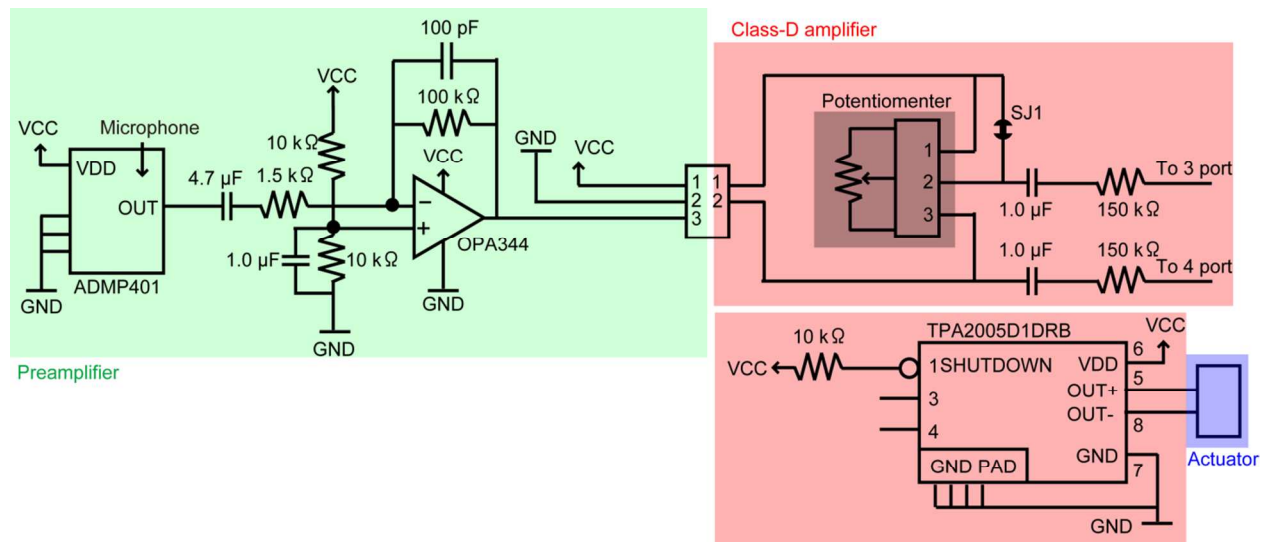
**Fig. S7. Circuit diagram of the signal-conditioning circuit for the bone-conduction hearing aid**
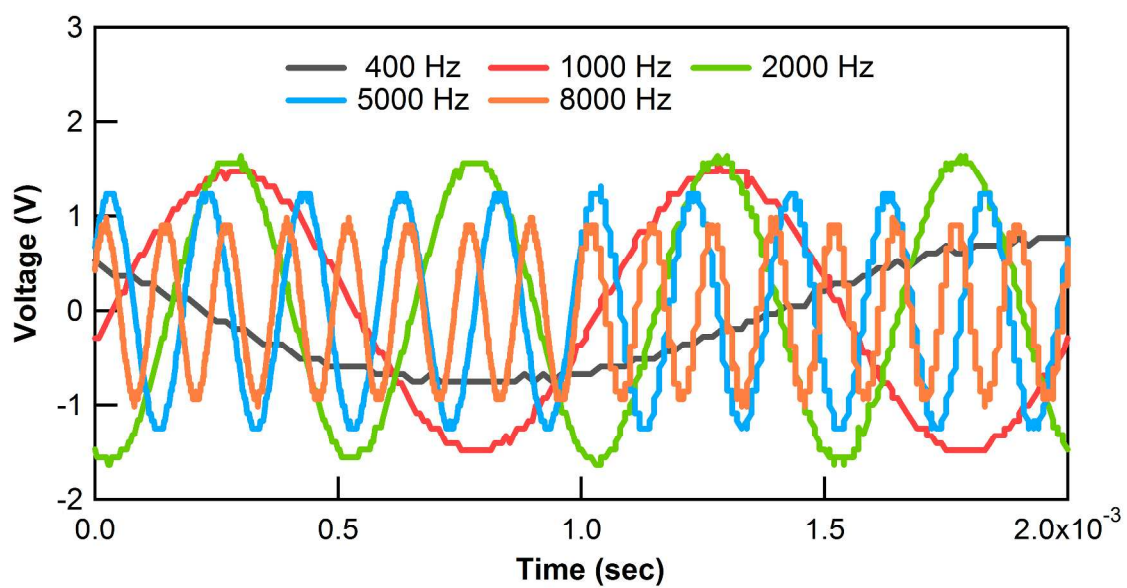
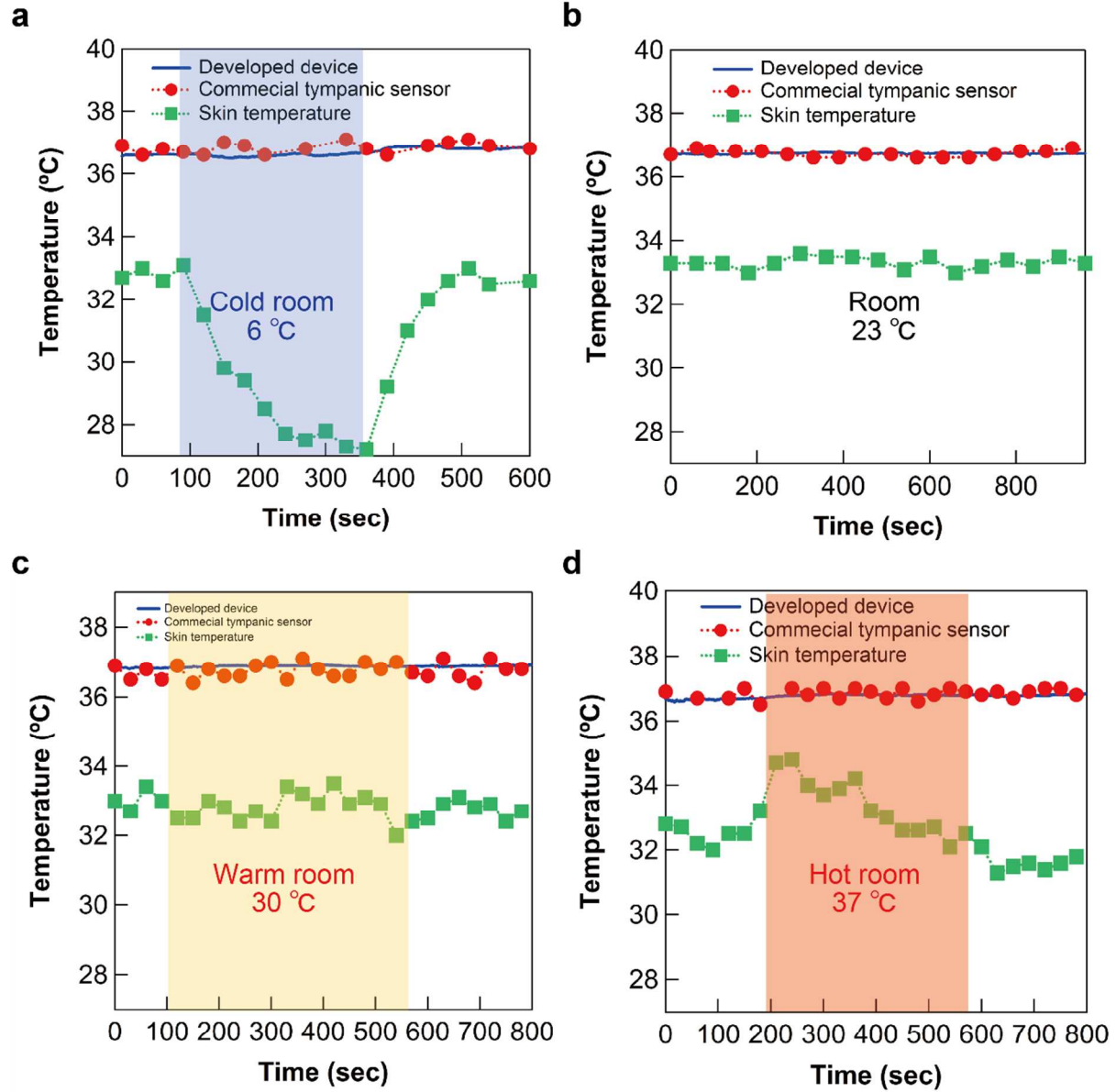**Fig. S8. Input voltages for the reference tones from a cell phone**

**Fig. S9. Skin and core body temperature change when a subject is exposed to rooms at 6(a), 23(b), 30(c), and 37 °C(d).**
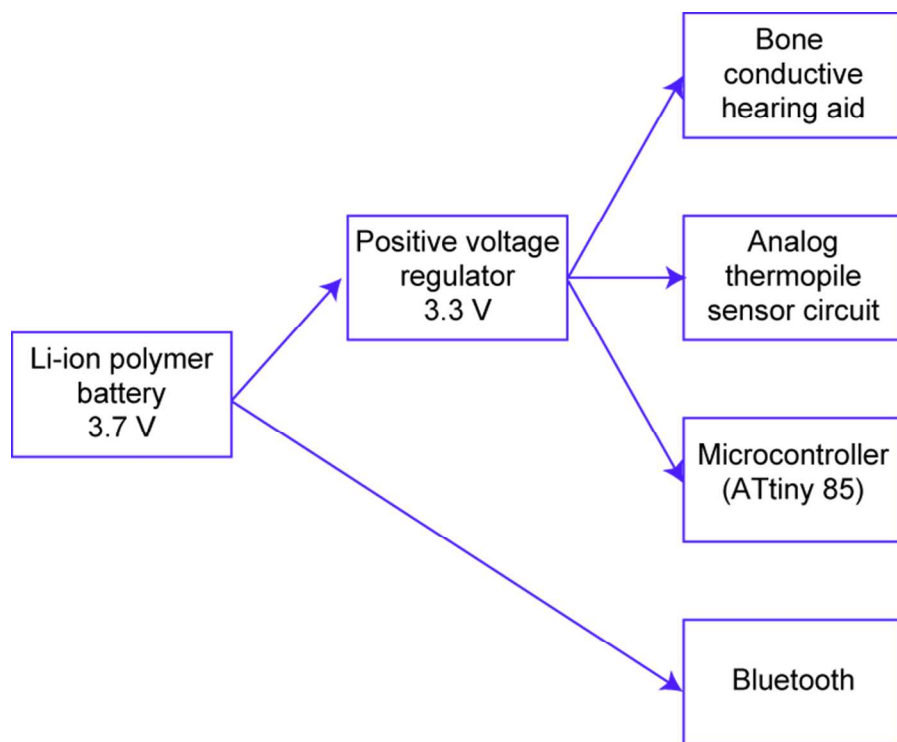
**Fig. S10. Power distribution of the 3.7 Li-ion polymer battery**